











Article

Photon-In/Photon-Out X-ray Free-Electron Laser Studies of Radiolysis

Linda Young^{1,2,*}, Emily T. Nienhuis³, Dimitris Koulentianos¹, Gilles Doumy¹, Anne Marie March¹, Stephen H. Southworth¹, Sue B. Clark^{3,4}, Thomas M. Orlando⁵, Jay A. LaVerne⁶ and Carolyn I. Pearce^{3,7,*}

- ¹ Chemical Sciences and Engineering Division, Argonne National Laboratory, Lemont, IL 60439, USA; koulentianos@anl.gov (D.K.); gdoumy@anl.gov (G.D.); amarch@anl.gov (A.M.M.); southworth@anl.gov (S.H.S.)
 - ² Department of Physics and James Franck Institute, The University of Chicago, Chicago, IL 60637, USA
 - ³ Pacific Northwest National Laboratory, Richland, WA 99354, USA; emily.nienhuis@pnnl.gov (E.T.N.); sue.clark@pnnl.gov (S.B.C.)
 - ⁴ Department of Chemistry, Washington State University, Pullman, WA 99164, USA
 - ⁵ Georgia Institute of Technology, School of Chemistry and Biochemistry, Atlanta, GA 30332, USA; thomas.orlando@chemistry.gatech.edu
 - ⁶ Radiation Laboratory and Department of Physics, University of Notre Dame, Notre Dame, IN 46556, USA; jay.a.laverne.1@nd.edu
 - ⁷ Department of Crop and Soil Sciences, Washington State University, Pullman, WA 99164, USA
- * Correspondence: young@anl.gov (L.Y.); carolyn.pearce@pnnl.gov (C.I.P.)

Abstract: Understanding the origin of reactive species following ionization in aqueous systems is an important aspect of radiation–matter interactions as the initial reactive species lead to production of radicals and subsequent long-term radiation damage. Tunable ultrafast X-ray free-electron pulses provide a new window to probe events occurring on the sub-picosecond timescale, supplementing other methodologies, such as pulse radiolysis, scavenger studies, and stop flow that capture longer timescale chemical phenomena. We review initial work capturing the fastest chemical processes in liquid water radiolysis using optical pump/X-ray probe spectroscopy in the water window and discuss how ultrafast X-ray pump/X-ray probe spectroscopies can examine ionization-induced processes more generally and with better time resolution. Ultimately, these methods will be applied to understanding radiation effects in complex aqueous solutions present in high-level nuclear waste.

Keywords: X-ray pump/X-ray probe; X-ray free-electron laser; water radiolysis; high-level nuclear waste



Citation: Young, L.; Nienhuis, E.T.; Koulentianos, D.; Doumy, G.; March, A.M.; Southworth, S.H.; Clark, S.B.; Orlando, T.M.; LaVerne, J.A.; Pearce, C.I. Photon-In/Photon-Out X-ray Free-Electron Laser Studies of Radiolysis. *Appl. Sci.* **2021**, *11*, 701. <http://doi.org/10.3390/app11020701>

Received: 23 December 2020

Accepted: 11 January 2021

Published: 13 January 2021

Publisher's Note: MDPI stays neutral with regard to jurisdictional claims in published maps and institutional affiliations.



Copyright: © 2021 by the authors. Licensee MDPI, Basel, Switzerland. This article is an open access article distributed under the terms and conditions of the Creative Commons Attribution (CC BY) license (<https://creativecommons.org/licenses/by/4.0/>).

1. Introduction

Understanding the elementary steps following ionization in aqueous systems will provide a framework for radiation–matter interactions in chemistry and biology. It is of central importance for radiobiological physics and chemistry and impacts cancer therapies, space travel, nuclear reactors, and environmental management [1,2]. Impact of an ionizing particle (X-ray, gamma, ion) leads to ejection of energetic primary electrons, followed by inelastic and non-adiabatic processes that produce highly damaging slower secondary electrons during the so-called physical and physico-chemical stages, that is, within a time scale of 10^{-12} s [1]. During these stages, reactive radical species are produced, e.g., the hydrated electron [3,4] and the chemically aggressive hydroxyl radical [5,6]. These radical species as well as H atoms and the molecular products H_2 and H_2O_2 will undergo reactions amongst themselves and with any added solutes, interfaces, etc. in the subsequent chemical stage to induce radiation damage that may not be manifest until even decades following the initial passage of the ionizing radiation. Although these latter reactions are nominally the observed outcome of radiolysis, it is the very fast processes on the sub-picosecond time scale that initiate this radiation damage.

Most studies in the ultrafast physico-chemical time regime of liquid water radiolysis have focused on the hydrated electron as summarized in a recent comprehensive review [4]. The primary ionization produces H_2O^+ and a quasifree electron. Only recently has the elementary proton transfer reaction $\text{H}_2\text{O}^+ + \text{H}_2\text{O} \rightarrow \text{H}_3\text{O}^+ + \text{OH}$, which occurs in ~ 50 -fs to produce the hydroxyl radical, been observed [5]. Generally speaking, experimental data probing the mechanisms of more complex chemical reactions on ultrafast timescales are extremely limited, despite being critical input for modeling of radiation chemistries, particularly in condensed phases.

Inner-shell vacancy decay represents a first step in radiation chemistries and in the condensed phase differs significantly from that of isolated atoms in the gas phase, where non-radiative Auger decay and fluorescence are well characterized. Following theoretical predictions [7] for inner-valence excitation, studies of gas-phase clusters have revealed a novel, non-local decay mechanism, Intermolecular Coulombic Decay (ICD) first in neon and water dimers [8,9]. In ICD, when the energy of the initially created hole is greater than the double ionization potential of the system, energy transfer following Auger-decay can eject an “ICD” electron from the neighbor of the originally excited molecule, leading to a Coulomb explosion and slow electrons that can be captured in coincidence with recoiling ions. Studies with larger clusters suggest that the propensity toward non-local decay increases with size [10].

Extensions to condensed phases have been pioneered using electron spectroscopy in liquid microjets by Winter and co-workers [11,12] and have been initiated by core level ionization. These studies have revealed other non-local decay mechanisms, e.g., electron transfer mediated decay (ETMD). Static electron spectroscopy measurements identified ETMD and ICD by lineshape analysis—observing subtle changes in Auger spectra and inferring time resolution using the internal Auger clock, ~ 4 fs for the oxygen 1 s hole. For example, comparison of the Auger spectra of normal and heavy water revealed that the inner-shell triggered autoionization processes are affected by proton transfer (OH stretching frequency is ~ 9 fs) [13]. It was noted that the experimental spectra alone provided limited insight into the type of the relaxation processes contributing to the spectrum, and no information on their relative efficiencies could be inferred because the kinetic energy released in the different relaxation channels is similar—*ab initio* theoretical calculations are essential for interpretation. It was shown that ICD occurs at condensed interfaces containing water by examining the protonated water cluster ion, kinetic energy release, and threshold production energy. The latter was correlated with *s*-shell ionization of rare gas partners. Though these experiments could clearly reveal the occurrence of ICD in complex condensed phase targets, they could not determine the time scales of the proton transfer step vs. the initiating ICD event [14]. In general, the temporal evolution of the transient species can not be extracted from static experimental spectra [15].

Going beyond static photoelectron spectroscopy, one may consider time-resolved photoelectron spectroscopy (TRPES) to probe atom-specific mechanistic details of ionization-induced reactions in solution. Such studies have focused on the hydrated electron, where the modest vertical binding energy (VBE) of ~ 3.5 eV allows detection in both the ground and excited states of e^- (aq) with readily available UV probes. As done previously for non-time-resolved studies of ICD [8,9], water cluster species introduced into vacuum in concert with ion/electron detection are often used to approximate bulk behavior [16–20]. TRPES studies in solution phase are challenging due to difficulties associated with introducing liquid jets [21] into the vacuum environment required by photoelectron spectrometers—space charge, electron escape depth issues render experimental realization and interpretation, respectively, a challenge [22]. The liquid jet studies have also focused on the dynamics of the hydrated electron; the e^- (aq) is created via a photoinduced charge transfer to solvent (CTTS) from a solute anion (I^- , Br^-) [23,24] and its dynamics subsequently studied with IR pump/UV probe spectroscopy with photoelectron detection.

Photon-in photon-out spectroscopies powered by soft X-ray free electron lasers (XFELs) provide a powerful window into aqueous phase chemical reactions in the physico-

chemical time domain. Not only is the few femtosecond time regime and the photon energy to probe inner-shell hole configurations of oxygen, the K-shell absorption edges of carbon (284 eV), nitrogen (410 eV), oxygen (543 eV) and aluminum (1560 eV) readily accessible, but the challenging vacuum requirement for photoelectron spectroscopy is markedly reduced. A further enabling breakthrough has been the development of stable liquid sheet jets of micron and sub-micron thickness [25,26]. This combination of soft X-ray XFELs and the liquid sheet jets has enabled laser-pump/X-ray probe time-resolved absorption spectroscopy in the soft X-ray water window (280–530 eV) with milliOD sensitivity [5] and time-resolved resonant inelastic X-ray scattering (RIXS) [6] to study the fastest chemical processes in water radiolysis.

Here we recap the optical pump/X-ray probe studies of radiolysis in pure liquid water in Section 2.1. In Section 2.2, we describe the prospects for extending these fundamental studies to the less “ideal” situation encountered in true radiolysis environments via X-ray pump/X-ray probe studies. In Section 2.3, we briefly describe methods used at longer timescales to probe radiolysis products, i.e., pulse radiolysis, scavenger, and stop-flow methods. In Section 3, we discuss the application to a practical problem of considerable importance: remediation of high-level nuclear waste (HLW). Finally in Section 4, we describe the outlook for ultrafast studies of radiolysis with XFELs.

2. Methods

As a prototype of radiation-induced chemical reactions in more complex systems, we first consider pure water radiolysis as shown in Figure 1. The physico-chemical time regime is covered primarily by XFEL pump/probe (and optical pump/probe studies, as described in the introduction). The tabletop optical pump/probe studies have been limited to the study of the hydrated electron with those in the bulk liquid studies often employing solute anions to generate e^- (aq), though extensions to the soft X-ray transient absorption studies are becoming feasible as high harmonic sources approach the oxygen K-edge [27–29]. Chemical phenomena occurring on longer timescales are addressed by pulse radiolysis, scavenger, and stopped flow techniques. The combination of these many methods promise a comprehensive view of ionization-induced phenomena in complex systems.

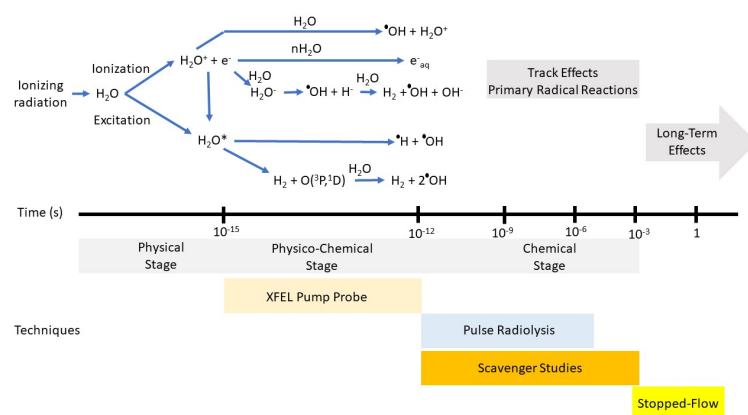


Figure 1. Top: Various stages that occur in the radiolysis of water by fast ions or electrons or energetic photons. Energy loss by the incident radiation to produce ionized or excited states of the medium is considered to occur in the physical stage that is best described in terms of cross sections. The relaxation of the medium from a few femtoseconds to about a picosecond is considered the physico-chemical stage and represents the true beginning of the formation of chemically reactive species and that can be examined by XFELs. From top to bottom, these processes following ionization of the water molecule are the proton transfer to produce the OH radical, hydration of the electron, and dissociative electron attachment. Neutralization of the electron with the water cation or direct excitation will lead to the excited water molecule followed by two most probable reactions shown. Reaction scheme and time scales taken from Ref. [30]. Bottom: Techniques used to probe chemical phenomena at various timescales.

The physico-chemical stage of the decomposition of pure water is independent of the radiation type. However, water in confined spaces or with high solute concentrations can have very different outcomes because of reactions within this time frame. Obviously, the transient species must be near its reaction site because mass diffusion does not occur on this timescale. Chemistry occurring on this timescale can be inferred by analysis of products at longer times, or, preferentially by examination of the variation in the temporal decay of the transient species using pump/probes technique with XFELs.

2.1. Optical-Pump/X-ray Probe

Understanding the birth and fate of an excess electron in liquid water created by ionization is a longstanding scientific problem addressed by ultrafast pump-probe techniques. Historically, all-optical techniques in liquid jets were employed using multiphoton [31–33] or two-photon ionization [34] to inject electrons and/or study the pre-equilibrated hydrated electron [35,36]. Surprisingly the partner in the initial ionization step, the H_2O^+ cation has remained undetected, despite a rigorous UV-pump/broadband UV-Vis probe study, due to its femtosecond lifetime and unclear spectroscopic signature in the UV/VIS region [37]. To this day, there are many unresolved questions associated with the hydrated electron in liquid water.

The advent of X-ray free electron lasers with intense, tunable soft X-ray pulses in the soft X-ray water window presented a new opportunity to probe the dynamics associated with valence holes created during ionization of water, enabling our recent experiment [5]. The strategy follows our earlier studies using X-rays to probe the residual ion following following strong-field ionization [38,39]. Our calculations demonstrate a clear signature for H_2O^+ and other relevant radiolysis species in the water window Figure 2. The absorption resonances in the gas phase for the four species associated with elementary proton transfer: $\text{H}_2\text{O}^+ + \text{H}_2\text{O} \rightarrow \text{OH} + \text{H}_3\text{O}^+$ were calculated with 6-311(2+,+)G(2df,p) basis with uncontracted core (oxygen) using fc-cvs-EOM-CCSD [40]. We used strong-field ionization in water (800 nm, $2 \times 10^{13} \text{ W/cm}^2$) [41] to impulsively eject an electron along the field polarization axis to a radius of 35 Å. The ejected electron ultimately equilibrates in a spherical solvent cavity of 3 Å in an s-like ground state within 1 ps. Prior to the equilibration of the hydrated electron, dynamics of the valence hole was probed with a delayed monochromatic X-ray pulse ($\tau_X = 20 \text{ fs}$, $\Delta E_X = 0.20 \text{ eV}$) scanned over the water window. Three detection channels were simultaneously observed: transmission, total fluorescence, and dispersed emission. The ability to vary the polarization of the optical strong-field pump relative to the linearly polarized X-ray probe between 0° and 90° allowed us to extract an isotropic transient absorption signal with milliOD sensitivity for an ionization fraction of roughly 1%. The isotropic transient absorption signal tuned directly to the OH(aq) resonance exhibited a delayed onset relative to X-ray probe energies to the red or blue, providing a signature for the ultrafast proton transfer reaction. The time resolution of these measurements was limited by the measurement of the time-delay between the optical pump and X-ray probe pulses to $\sim 100 \text{ fs}$. Importantly, our theoretical quantum mechanics/molecular mechanics (QM/MM) results showed the sensitivity of the valence hole X-ray absorption to the structural dynamics around the ionization site, particularly the O-O distance to the nearest neighbor H_2O , with 0.2 eV shifts corresponding to $\sim 0.2 \text{ \AA}$ changes.

The dispersed emission channel mapped inelastic X-ray scattering as a function of incoming photon energy [6]. When the incoming photon energy is tuned to the OH(aq) resonance, resonant inelastic X-ray scattering (RIXS) of the transient radical is observed. Simultaneous detection of RIXS and transient absorption was achieved by setting the 2.0 μm sheet jet at a 45° angle to the incoming X-ray beam. Although collection/detection efficiency was poor in this channel ($\sim 10^{-8}$), statistics accumulated by averaging for pump-probe delay times $>200 \text{ fs}$ allowed the extraction of an RIXS signal. This RIXS signal showed the ability of the dispersed X-ray emission to report on local electronic transitions of the hydroxyl radical solute, unlike UV absorption spectroscopies where charge transfer transi-

tions dominate, and thereby provide another characterization tool for ultrafast chemical reactions in solution.

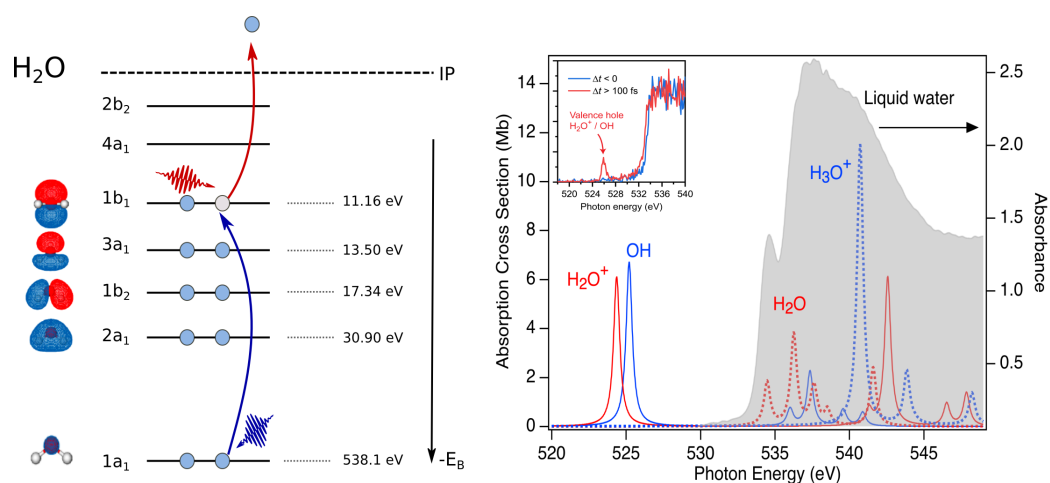


Figure 2. Schematic of optical pump/X-ray probe transient absorption study of water radiolysis. Left: Strong-field laser pump (red photon) ejects an electron from the outermost $1b_1$ orbital. X-ray probe (blue photon) induces the transition from the core $1s$ level to the vacancy in the $1b_1$ ($1a_1 \rightarrow 1b_1$). Right: Absorption spectrum of liquid water for a thickness of 800 nm [42] in gray. Calculated gas phase absorption for H_2O^+ and OH. Liquid phase binding energies for electrons in the various orbitals [43]. Inset shows the experimental X-ray transient absorption spectrum of the OH(aq) radical. Reproduced from Reference [5].

2.2. X-ray Pump/X-ray Probe

We now step beyond the ideal case created by impulsive strong-field ionization, i.e., a single ejected electron and a valence hole—basically an electron–hole pair in water—to the situation created by passage of an ionizing X-ray pulse. The X-ray pump/X-ray probe method allows us to extend our earlier study in two important dimensions. First, whereas our previous studies [5,6] focused on the elementary electron–hole dynamics associated with strong-field ionization from the HOMO in pure liquid water, here we can access ionization from any orbital—more directly mimicking early events in actual radiolysis. Second, the time resolution associated with the earlier study was limited to ~ 100 fs, much too slow to capture correlated hole–proton motions in water, whereas this new X-ray pump/X-ray probe scheme offers sub-femtosecond time-resolution between pump and probe. We note that water is also an excellent testbed for studies of coupled electron–nuclear motion as spatial correlations between nuclear displacement of a light proton and hole can be large [44].

The powerful two-color X-ray pump/X-ray probe schemes at the Linac Coherent Light Source (LCLS) of Stanford Linear Accelerator Center (SLAC) National Accelerator Laboratory [45–47] provide the means to systematically understand the electronic and nuclear dynamics following valence, inner-valence and core ionization in aqueous systems (Figure 3). An X-ray pump pulse with a photon energy below the $1s$ ionization threshold (538.1 eV) can non-resonantly create a hole in any of the valence or inner valence bands, as indicated by the green photons. An X-ray probe pulse can be tuned to selectively probe the dynamics of individual hole states ($1b_2$, $3a_1$, $1b_1$) as shown on the left side of Figure 3. The predicted separation of absorption bands is given by the differences in their binding energies in the liquid phase [43]. Based upon estimated oscillator strengths for the $1s$ transitions to valence hole states, the estimated absorption spectrum is constructed, as shown in the right panel of Figure 3. The relatively small oscillator strength for the $1s_1 \rightarrow 2a_1$ transition is due to dipole selection rules and the symmetries of the respective orbitals.

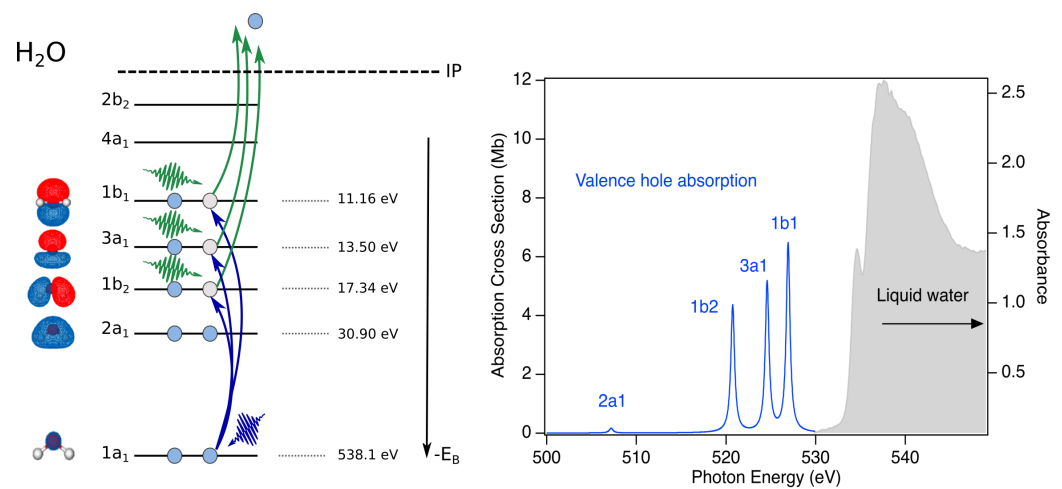


Figure 3. Schematic of a potential X-ray pump/X-ray probe transient absorption study of water radiolysis. Left: X-ray pump photons (green) eject an electron from any of the valence or inner-valence orbitals $1b_1$, $3a_1$, $1b_2$, $2a_1$. X-ray probe photons (blue) selectively induces transitions from the $1s$ core level to the vacancies, (e.g., $1a_1 \rightarrow 1b_2$). Right: Absorption spectrum of liquid water for a thickness of 800 nm [42] in solid gray. Calculated positions for absorption based upon the liquid phase binding energies [43]. The several eV separation of the bands allows to distinguish hole dynamics in different orbitals.

A schematic of a straightforward X-ray pump/X-ray probe transient absorption configuration is shown in Figure 4. Two independently controlled X-ray pulses with arbitrary central wavelength (250–1600 eV) and pulse delay (0–100 fs) can now be generated at LCLS with the new variable gap soft X-ray undulators and a magnetic chicane located after the eighth undulator. The pulse duration can be adjusted to a few femtoseconds using either low electron bunch charge or an emittance spoiler [48]. While the X-ray bandwidth in self-amplified spontaneous emission (SASE) mode is typically 1% of the central photon energy, and ΔE_X can be both broader and smoother using the X-ray laser enhanced attosecond pulse (XLEAP) configuration [47], the actual resolution of the transient absorption spectrum will be set by the design of the grating spectrograph—which, for this first application, requires only a moderate resolution of $1/3000$ [49]. Normalization of the incident pulse energy is expected on a shot-by-shot basis at the 1% level using extensions of fluorescence intensity monitoring [50].

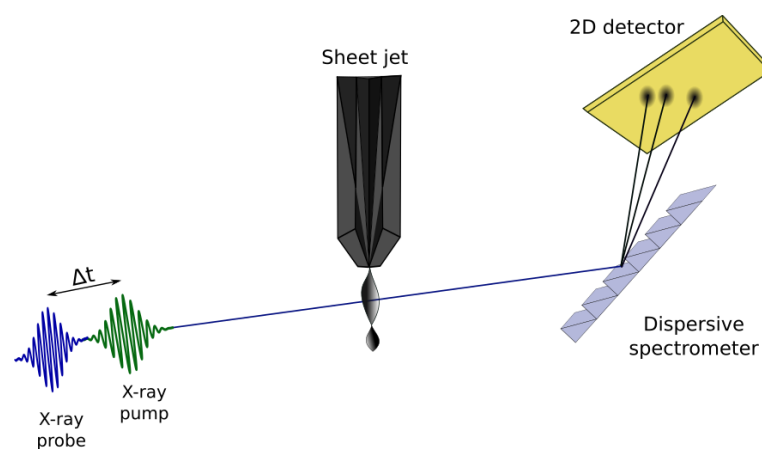


Figure 4. Simplified schematic of an X-ray pump/X-ray probe transient absorption experimental setup to study water radiolysis. Two broad bandwidth X-ray pulses, pump (green) and probe (blue) are produced collinearly from the accelerator and overlapped in a thin liquid sheet jet. Pump/probe delays between 0–100 fs are set with attosecond precision by the magnetic chicane. The transmitted beam is energy dispersed with a grating and detected on a 2D pixel array.

It is desirable to study radiolysis in the isolated event regime. The concentration of ionization events can be readily controlled by the fluence of the X-ray pump pulses, i.e., the pulse energy/focal spot area. An additional consideration is to remain in the linear regime of X-ray interactions. As an example, for a pump pulse energy of 5 μJ on target at 260 eV, water jet thickness of 0.4 μm , spot area of 100 μm^2 , one obtains an ionization fraction of 2% and a transmission of 77%. The relatively large area of the converging sheet jet (1 \times 3 mm, H \times V) can accommodate a substantial defocusing from the above size to achieve isolated event conditions. Our earlier X-ray transient absorption studies operated with an ionization fraction of <1% and observed a change in absorption of \sim 10% for the analogous $1a_1 \rightarrow 1b_1$ transition—validating the feasibility of the X-ray pump/X-ray probe approach for studies of the physico-chemical timescale of water radiolysis.

2.3. Chemical Stage Methods

Many studies have been published on examination of the long-term radiation effects and date from original experiments in the Curie laboratories [51]. These experiments examine the production of final products with no direct determination of the mechanism. Reactions leading to the observed products can be inferred by using competition kinetics. For instance, solutions are commonly saturated with N_2O to convert the hydrated electron to the OH radical. A decrease in product yield would infer there was a hydrated electron intermediate while a doubling of the yield indicates the OH radical is important. Solutes that trap free radicals can be used to probe their role in the radiolysis process. Many clever uses of competition kinetics have been invoked over the decades to infer the reactions of intermediates occurring in the chemical stage.

The sophistication for probing the chemical stage has advanced as technology has developed. The most significant advance for direct observation of the transient species was the development of pulse radiolysis in the 1960s. These early instruments were electron accelerator based with resolution on the microsecond time scale [52–54]. They used thermal-based electron cathodes to make pulses of sufficient intensity that the transients could be examined using optical detection techniques. Many of these early studies focused on reactions of the hydrated electron because of its relatively large extinction coefficient [2–4]. Inherent jitter in the timing of the cathode pulse with detectors limited these instruments to the nanosecond time scale. Pulse radiolysis on the picosecond time domain came with the adoption of laser driven cathodes in which optical detectors could be inherently correlated to pulse formation [55,56]. These latter techniques greatly increased knowledge on the reactions of transients in the chemical stage. Examination of processes occurring in the chemical stage is now limited by appropriate detectors. However, present pulse radiolysis techniques are still insufficient to examine initial water decomposition. Probing the physico-chemical stage using pulse radiolysis is again limited to indirect techniques. For instance, the concentration of solutes with high reactivity to the precursor to the hydrated electron can be varied while observing the picosecond yield of the hydrated electron to give an indication of the underlying kinetics.

3. Discussion and Applications

Foundational studies of radiolysis in pure water on the physico-chemical timescale provide the necessary background to pursue such processes in more complex systems—including those relevant for management of legacy wastes from nuclear technologies. This includes spent nuclear fuels from reactors, and wastes generated from processing of nuclear materials. Many of these materials are oxides and oxyhydroxides of elements, such as aluminum, that were present in the nuclear systems. For the case of certain specialized spent nuclear fuels (SNF), aluminum was used as cladding. The US government manages more than 10 metric tons of these specialized SNF assemblies, and long-term storage has led to cladding corrosion and the formation of aluminum hydroxide/oxyhydroxide hydrate layers. Radiolysis of the water associated with these materials drives the formation

of molecular hydrogen and other byproducts that must be quantified and considered in decisions regarding their long-term storage.

In the situation of wastes from nuclear materials processing, the production of plutonium from irradiated targets has resulted in the generation of more than 300 million liters of high-level radioactive wastes stored in underground tanks that must be managed by the Department of Energy's Office of Environmental Management (EM) [57]. The Hanford site in Washington State, USA houses 54 million gallons of hazardous radioactive waste, categorized as high-level waste (HLW) or low activity waste (LAW), resulting from decades of plutonium production, and currently stored in 177 underground steel tanks. The tank waste chemistry is complex (Figure 5a) and it consists of an aqueous supernatant, salt cake solids, and a sludge layer [58]. The supernatant liquid is a caustic mixture of 3–5 molar sodium hydroxide (NaOH) and large fractions of oxyanions, such as nitrate (NO_3^-) and nitrite (NO_2^-), with the dominant metallic element being aluminum (Al). The salt cake consists of water-soluble oxyanion and halide salts. The sludge consists primarily of insoluble Al oxides and oxyhydroxides, such as gibbsite ($\text{Al}(\text{OH})_3$), or amorphous agglomerates of varying sizes and morphologies, all of which serve to complicate retrieval and processing [58,59].

The tank waste will be retrieved and processed into a chemically durable vitrified waste form for final disposal [60]. This remediation effort hinges on understanding components present in both the solid and aqueous phase, and controlling dissolution, precipitation, and particle aggregation reactions [61]. Foundational to this is a complete understanding of radiation-driven reactions and their implications for the speciation, structure, and dynamics of solutions representative of the waste.

Within the tanks, γ -ray and β emitters are the primary radiation load (^{137}Cs , ^{90}Sr , ^{99}Tc , ^{129}I) [60,62,63]. Many of these radionuclides are present in the supernatant but can also be present in the tank sludge [63], potentially impacting solution speciation and structure, as well as aggregation behavior and solubility of the solid phases. Though γ -radiation is the primary radiation load for the chemically complex tank wastes, to better understand the impacts, different radiation sources are being used to evaluate the various timescales and processes in simplified solutions representative of the major components of the waste, such as is shown in the $\text{Na}_2\text{O}-\text{Al}_2\text{O}_3-\text{H}_2\text{O}$ ternary phase diagram in Figure 5b. Future work will place greater emphasis on increasingly complex electrolyte solutions to be more representative of simulant tank wastes, and the cascade of processes across broad time and length scales that are set in motion by ionizing radiation.

Gamma rays, the primary radiation load in HLW, interact with water in a Compton process in which the incident photon behaves as a particle to produce an electron of a few hundred keV. Radiolysis of water by gamma rays is indistinguishable from that by fast electrons. The initial energy loss by fast charged particles to a medium water molecule can vary widely according to kinematic limits, but the average energy loss is about 60 eV. This average is nearly constant and independent of the initial energy of electrons and heavy ions [64]. A 60 eV electron will scatter significantly along its path as it produces a series of lower energy ionization events. The result is a localized cluster or spur of ionized and excited water molecules that will decay as described above in the physico-chemical stage. Each initial event is a stochastic process so the number of ionized and excited water molecules in a spur varies from about one to six [65]. The true chemical stage starts at about 100 picoseconds when diffusion begins and lasts until about a microsecond. During this period the reactions of the sibling products within a spur will react and diffuse as the non-homogeneous spur decays. Heavy ions have a much higher rate of energy loss than electron so the spurs overlap to form a track. Track effects generally describe the chemical stage for fast electrons and heavy ions and the competition between reaction and diffusion is responsible for the observed difference in product yields. A variety of time resolved techniques are available for directly probing the temporal variation of radicals in the radiolysis of water during the chemical stage. Pulse radiolysis with electrons in the MeV energy range can use a variety of optical detection techniques to directly probe radical

reactions. The single pulse dose from the sources is considerably greater than typically found with gamma rays but the results are expected to be the same.

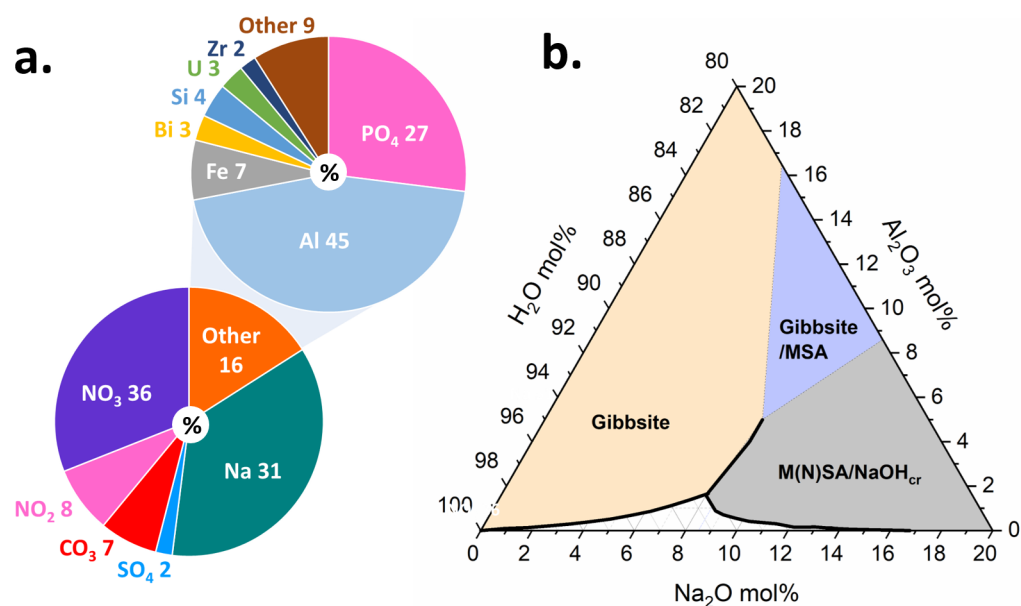


Figure 5. (a) Composition estimate for Hanford tank waste, which shows relatively high proportions of Na and Al. Data adapted from Ref. [66]. The composition of the waste can promote crystallization and aggregation of Al hydroxides. (b) Na₂O-Al₂O₃-H₂O ternary phase diagram showing solubility region as well as regions saturated with respect to gibbsite, gibbsite/monosodium aluminate hydrate, and monosodium aluminate hydrate/nonasodium bis(hexahydroxyaluminate) trihydroxide hexahydrate/sodium hydroxide. Data adapted from Refs. [67–69]. The composition of the tank waste promotes formation of some of these species. While previous radiolysis studies have focused on pure water, future studies will increase in complexity and explore compositions within the phase diagram.

Long-term effects are considered to be due to reactions of radicals with solutes or at interfaces near to the water medium. Variations in radical yields and thereby long-term effects are dependent on the number of radicals produced in the physico-chemical stage as well as the subsequent track chemistry in the chemical stage. Examination of radiation effects on long time scales can utilize any number of standard spectroscopic or chromatographic techniques.

Gamma rays are impractical for examination of real-time radical chemistry because they are continuous in nature. However, scavenging techniques are ideally suitable for use with continuous radiation sources. In addition, scavenging techniques can be used over an incredibly wide range of times. This technique makes use of a solute, scavenger, to react with a specific radical to give a measurable stable product. The scavenging capacity is defined as the product of the scavenger concentration and the rate coefficient for the scavenging reaction and represents the inverse of the lifetime of the radical. Observation of final product yields with variation of the scavenger concentration is a simple technique for estimating the radical kinetics. An even more sophisticated approach utilizes the relationship that the inverse Laplace transform of the scavenging capacity dependence directly gives the time dependence of the scavenged radical [70]. Scavenging techniques are commonly used where pulse radiolysis cannot be used as in gamma or heavy ion radiolysis. Several studies have shown that scavenger techniques are reliable to give real time information on radical chemistry [70].

As discussed above for pure water solutions, complex solutions containing solvated ions and ionic solids such as metal-oxides also undergo intra- and inter-atomic Auger decay and possibly ICD and ETMD involving the interfacial water molecules. A recent low-energy electron scattering study that simulates the secondary electron interactions

from X-rays and high energy gamma rays, demonstrated very efficient ICD and ETMD in micro-solvated boehmite (AlOOH) nanoplatelets [71]. This occurs when the density of states of the ionized chemisorbed species significantly overlaps the core hole states of the solid and is likely a primary process for producing ionized and radical species at the interfaces of particles in complex waste forms. This experimental and theoretical work demonstrated that ICD is a preferred decay mechanism upon single and double shallow core hole excitation of adsorbed interfacial water and the underlying nanoplatelet. ETMD from the water also occurs following ionization of the boehmite Al(2s) level. ICD and ETMD both lead to the formation and ejection of H_2O^+ with broad bimodal kinetic energy release (KER) distributions. The latter indicates the involvement of a manifold of complex multi-hole states with lifetimes that compete with proton transfer and hole delocalization. None of these interactions have been probed with time-resolved techniques,

In solutions where solute species are present, there will be radiation-induced changes to the subsequent reaction pathways and reaction timelines [72]. As an example, see Figure 6. Production of these additional species takes place through relaxation processes, such as ETMD and ICD. For example, ICD can create final states of $\text{M}^{(q+1)+} \cdot \text{H}_2\text{O}^+$ and ETMD can create $\text{M}^q \cdot \text{H}_2\text{O}_2^+$ within the first solvent shell around the reactive site [72]. In the case of water, H_2O^+ leads to a proton transfer reaction that generates an OH^\bullet radical. ICD and ETMD are competitive processes, with their relative importance in aqueous ionic solutions depending on the ion charge state, polarizability, and geometric structure of the solvent shell. Although the interactions are localized, the lifetimes depend on the number of water molecules involved and the distance from the central metal atom, and we hypothesize that there will be significant differences between alkaline systems and that observed in water; the central $\text{Na}^+ - \text{O}$ distance aqueous solution is 2.377 Å vs. 2.604 Å for the O—O distance in water.

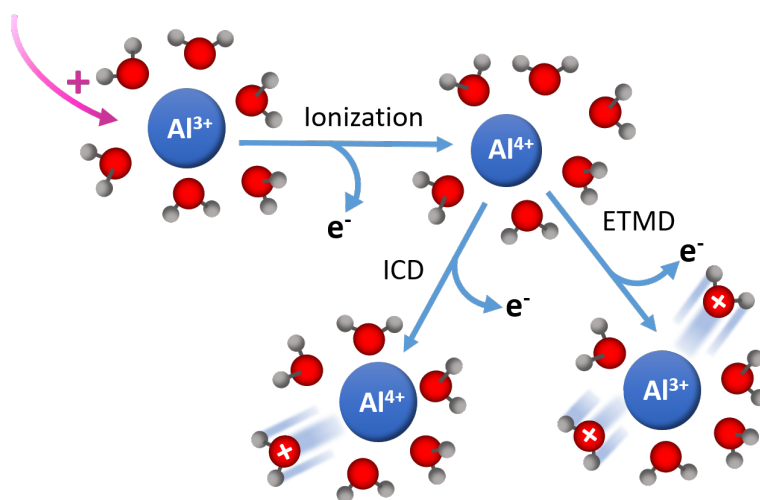


Figure 6. Ultrafast X-ray spectroscopies represent a new tool to understand the initial mechanisms that produce reactive species. Tunability throughout the soft-X-ray range allows access to important elemental species such as oxygen, nitrogen, and aluminum, of which, are of utmost importance for understanding these processes in high-level waste. For example, in complex solutions, alternative decay channels, such as ICD and ETMD, become operative. Shown here is the case for Al^{3+} surrounded by H_2O . In the case of concentrated solutions where ion-pairing may become prevalent, nearest neighbors may not be H_2O , which could further serve to alter the production of reactive species through ionization.

We plan to apply methodology similar to that used to study ultrafast radiolysis in water to a series of $\text{NaOH-H}_2\text{O}$ solutions, and later, expand the technique to more complex aluminate-containing solutions. To explore the earliest time events in radiation effects, we propose initially to use X-ray pump-probe experiments in water and $\text{NaOH-H}_2\text{O}$ solutions to look at the formation of reactive species and transients in the water window near the O

K-edge using the techniques developed for water ionization studies [5]. Though the NaOH components will not be observed directly in this manner, the way in which they perturb the water network will be. Analogously, the oxidation state of the Na can be independently probed on the ultrafast timescale giving a direct view into non-local decay processes at the metal-ion site. The specific questions we seek to answer include the impact of incomplete solvent shells as the nearest neighbors for ICD and ETMD processes are not necessarily a water molecule, the impact of ion networks on these processes when comparing dilute and concentrated solutions of similar composition, and the overall timescale of the processes resulting from alteration of the solution structure.

Interpretation of ultrafast X-ray spectroscopic measurements is invariably linked with theory, which, for understanding structural dynamics of core-excited matter, is an ongoing challenge as described in some recent reviews [73,74]. There are already challenges at a very basic level, e.g., to predict the X-ray absorption spectrum of ground-state species with sub-eV accuracy [75] and to locate the positions of double-hole states [76]. Here, advances in equation-of-motion coupled-cluster (EOM-CC) approaches [77,78] have allowed a systematic convergence after application of the core-valence separation scheme [79] within the EOM-CC framework [80]. This general approach has allowed EOM-CC-CVS to achieve improved accuracy for single photon transitions [40,81] and expand to two-photon RIXS calculations [82]. Beyond high-level calculations of electronic structure, capturing core-excited state dynamics poses a further challenge that has been largely pursued with simpler electronic structure methods [72,83,84]. Describing non-local multiple-hole dynamics in complex systems is likely to remain a frontier and foster synergistic research between experiment and theory.

4. Conclusions and Outlook

XFEL-based photon-in/photon-out spectroscopies represent an emerging and unique opportunity to study radiolysis in the sub-picosecond physico-chemical time range. For studies in the liquid phase, the photon-in/photon-out methods provide substantially relaxed vacuum requirements relative to those for the photoelectron-based spectroscopies. The versatile two-color, sub-femtosecond pulse generation capabilities over a wide energy range (250–1600 eV) at LCLS allow selection of initial ionization conditions and selective probing of ionization-generated chemical species by transient absorption. Similar capabilities are currently being considered at other facilities [85,86]. Advanced beamsplitter techniques that simultaneously provide sample and reference probe beams onto a single 2D-detector promise to further enhance the sensitivity for transient absorption studies [87,88]. The incorporation of RIXS further discriminates transient species with overlapping absorption resonances, and while statistically limited at present 120 Hz repetition rates, will become more routine at the MHz repetition rates soon expected. Such experimental studies can provide missing input into the challenging theoretical problem associated with the description of coupled electron-nuclear motion on highly excited electronic states associated with radiolysis in both simple and complex systems.

Author Contributions: Conceptualization, L.Y., E.T.N., J.A.L., and C.I.P.; methodology, L.Y., G.D., D.K., S.H.S., and A.M.M.; writing—original draft preparation, L.Y., E.T.N., D.K., J.A.L., and C.I.P. writing—review & editing, S.B.C., T.M.O. All authors have read and agreed to the published version of the manuscript.

Funding: This research was supported by IDREAM (Interfacial Dynamics in Radioactive Environments and Materials), an Energy Frontier Research Center funded by the U.S. Department of Energy (DOE), Office of Science, Basic Energy Sciences (BES). PNNL is a multiprogram national laboratory operated for DOE by Battelle Memorial Institute under Contract DE-AC05-76RL0-1830. DK,GD,AMM,SHS were supported by the U.S. Department of Energy, Office of Science, Basic Energy Science, Chemical Sciences, Geosciences, and Biosciences Division under Contract No. DE-AC02-06CH11357.

Institutional Review Board Statement: Not applicable.

Informed Consent Statement: Not applicable.

Data Availability Statement: The data presented in this study are available on request from the corresponding author.

Acknowledgments: We are grateful for technical discussions on the performance of LCLS operating modes with A. Marinelli, J. Cryan, on potential beamline and liquid jet endstation configurations with W.S. Schlotter, K. Kunnus, G. Dakovski, D. DePonte, M. Minitti, R.W. Schoenlein. We appreciate ongoing scientific discussions with Z.-H. Loh, J.-E. Rubensson and theoretical support from R. Santra, L. Inhester, A. I. Krylov, K. Nanda, L. Cheng, P.J. Ho, A. Fouda, X. Li, and A. Clark.

Conflicts of Interest: The authors declare no conflict of interest.

References

1. Alizadeh, E.; Sanche, L. Precursors of Solvated Electrons in Radiobiological Physics and Chemistry. *Chem. Rev.* **2012**, *112*, 5578–5602. [[CrossRef](#)] [[PubMed](#)]
2. Garrett, B.C.; Dixon, D.A.; Camaioni, D.M.; Chipman, D.M.; Johnson, M.A.; Jonah, C.D.; Kimmel, G.A.; Miller, J.H.; Rescigno, T.N.; Rosicky, P.J.; et al. Role of Water in Electron-Initiated Processes and Radical Chemistry: Issues and Scientific Advances. *Chem. Rev.* **2005**, *105*, 355–390. [[CrossRef](#)] [[PubMed](#)]
3. Hart, E.J.; Boag, J.W. Absorption Spectrum of the Hydrated Electron in Water and in Aqueous Solutions. *J. Am. Chem. Soc.* **1962**, *84*, 4090–4095. [[CrossRef](#)]
4. Herbert, J.M.; Coons, M.P. The Hydrated Electron. *Annu. Rev. Phys. Chem.* **2017**, *68*, 447–472. [[CrossRef](#)]
5. Loh, Z.H.; Doumy, G.; Arnold, C.; Kjellsson, L.; Southworth, S.H.; Al Haddad, A.; Kumagai, Y.; Tu, M.F.; Ho, P.J.; March, A.M.; et al. Observation of the fastest chemical processes in the radiolysis of water. *Science* **2020**, *367*, 179–182. [[CrossRef](#)]
6. Kjellsson, L.; Nanda, K.D.; Rubensson, J.E.; Doumy, G.; Southworth, S.H.; Ho, P.J.; March, A.M.; Al Haddad, A.; Kumagai, Y.; Tu, M.F.; et al. Resonant Inelastic X-ray Scattering Reveals Hidden Local Transitions of the Aqueous OH Radical. *Phys. Rev. Lett.* **2020**, *124*, 236001. [[CrossRef](#)]
7. Cederbaum, L.S.; Zobeley, J.; Tarantelli, F. Giant Intermolecular Decay and Fragmentation of Clusters. *Phys. Rev. Lett.* **1997**, *79*, 4778–4781. [[CrossRef](#)]
8. Jahnke, T.; Czasch, A.; Schöffler, M.S.; Schössler, S.; Knapp, A.; Kász, M.; Titze, J.; Wimmer, C.; Kreidi, K.; Grisenti, R.E.; Staudte, A.; et al. Experimental Observation of Interatomic Coulombic Decay in Neon Dimers. *Phys. Rev. Lett.* **2004**, *93*, 163401. [[CrossRef](#)]
9. Mucke, M.; Braune, M.; Barth, S.; Förstel, M.; Lischke, T.; Ulrich, V.; Arion, T.; Becker, U.; Bradshaw, A.; Hergenbahn, U. A hitherto unrecognized source of low-energy electrons in water. *Nat. Phys.* **2010**, *6*, 143–146. [[CrossRef](#)]
10. Richter, C.; Hollas, D.; Saak, C.M.; Förstel, M.; Miteva, T.; Mucke, M.; Björneholm, O.; Sisourat, N.; Slavíček, P.; Hergenbahn, U. Competition between proton transfer and intermolecular Coulombic decay in water. *Nat. Commun.* **2018**, *9*, 4988. [[CrossRef](#)]
11. Aziz, E.F.; Ottosson, N.; Faubel, M.; Hertel, I.V.; Winter, B. Interaction between liquid water and hydroxide revealed by core-hole de-excitation. *Nature* **2008**, *455*, 89–91. [[CrossRef](#)] [[PubMed](#)]
12. Thürmer, S.; Ončák, M.; Ottosson, N.; Seidel, R.; Hergenbahn, U.; Bradforth, S.E.; Slavíček, P.; Winter, B. On the nature and origin of dicationic, charge-separated species formed in liquid water on X-ray irradiation. *Nat. Chem.* **2013**, *5*, 590–596. [[CrossRef](#)] [[PubMed](#)]
13. Slavíček, P.; Winter, B.; Cederbaum, L.S.; Kryzhevoi, N.V. Proton-Transfer Mediated Enhancement of Nonlocal Electronic Relaxation Processes in X-ray Irradiated Liquid Water. *J. Am. Chem. Soc.* **2014**, *136*, 18170–18176. [[CrossRef](#)]
14. Grieves, G.A.; Orlando, T.M. Intermolecular Coulomb Decay at Weakly Coupled Heterogeneous Interfaces. *Phys. Rev. Lett.* **2011**, *107*, 016104. [[CrossRef](#)]
15. Slavíček, P.; Kryzhevoi, N.V.; Aziz, E.F.; Winter, B. Relaxation Processes in Aqueous Systems upon X-ray Ionization: Entanglement of Electronic and Nuclear Dynamics. *J. Phys. Chem. Lett.* **2016**, *7*, 234–243. [[CrossRef](#)] [[PubMed](#)]
16. Coe, J.V.; Lee, G.H.; Eaton, J.G.; Arnold, S.T.; Sarkas, H.W.; Bowen, K.H.; Ludewigt, C.; Haberland, H.; Worsnop, D.R. Photoelectron spectroscopy of hydrated electron cluster anions, $(\text{H}_2\text{O})^-_{n=2-69}$. *J. Chem. Phys.* **1990**, *92*, 3980–3982. [[CrossRef](#)]
17. Bragg, A.E.; Verlet, J.R.R.; Kammrath, A.; Cheshnovsky, O.; Neumark, D.M. Hydrated Electron Dynamics: From Clusters to Bulk. *Science* **2004**, *306*, 669–671. [[CrossRef](#)]
18. Coe, J.V.; Williams, S.M.; Bowen, K.H. Photoelectron spectra of hydrated electron clusters vs. cluster size: connecting to bulk. *Int. Rev. Phys. Chem.* **2008**, *27*, 27–51. [[CrossRef](#)]
19. Svoboda, V.; Michiels, R.; LaForge, A.C.; Med, J.; Stienkemeier, F.; Slavíček, P.; Wörner, H.J. Real-time observation of water radiolysis and hydrated electron formation induced by extreme-ultraviolet pulses. *Sci. Adv.* **2020**, *6*. [[CrossRef](#)]
20. LaForge, A.C.; Michiels, R.; Bohlen, M.; Callegari, C.; Clark, A.; von Conta, A.; Coreno, M.; Di Fraia, M.; Drabbels, M.; Huppert, M.; et al. Real-Time Dynamics of the Formation of Hydrated Electrons upon Irradiation of Water Clusters with Extreme Ultraviolet Light. *Phys. Rev. Lett.* **2019**, *122*, 133001. [[CrossRef](#)]

21. Winter, B.; Faubel, M.; Hertel, I.V.; Pettenkofer, C.; Bradforth, S.E.; Jagoda-Cwiklik, B.; Cwiklik, L.; Jungwirth, P. Electron Binding Energies of Hydrated H_3O^+ and OH^- : Photoelectron Spectroscopy of Aqueous Acid and Base Solutions Combined with Electronic Structure Calculations. *J. Am. Chem. Soc.* **2006**, *128*, 3864–3865. [[CrossRef](#)]
22. Suzuki, T. Time-resolved photoelectron spectroscopy of non-adiabatic electronic dynamics in gas and liquid phases. *Int. Rev. Phys. Chem.* **2012**, *31*, 265–318. [[CrossRef](#)]
23. Elkins, M.H.; Williams, H.L.; Shreve, A.T.; Neumark, D.M. Relaxation Mechanism of the Hydrated Electron. *Science* **2013**, *342*, 1496–1499. [[CrossRef](#)] [[PubMed](#)]
24. Karashima, S.; Yamamoto, Y.; Suzuki, T. Resolving Nonadiabatic Dynamics of Hydrated Electrons Using Ultrafast Photoemission Anisotropy. *Phys. Rev. Lett.* **2016**, *116*, 137601. [[CrossRef](#)] [[PubMed](#)]
25. Koralek, J.D.; Kim, J.B.; Brůža, P.; Curry, C.B.; Chen, Z.; Bechtel, H.A.; Cordones, A.A.; Sperling, P.; Toleikis, S.; Kern, J.F.; et al. Generation and characterization of ultrathin free-flowing liquid sheets. *Nat. Commun.* **2018**, *9*, 1353. [[CrossRef](#)] [[PubMed](#)]
26. Ha, B.; DePonte, D.P.; Santiago, J.G. Device design and flow scaling for liquid sheet jets. *Phys. Rev. Fluids* **2018**, *3*, 114202. [[CrossRef](#)]
27. Kraus, P.M.; Zürich, M.; Cushing, S.K.; Neumark, D.M.; Leone, S.R. The ultrafast X-ray spectroscopic revolution in chemical dynamics. *Nat. Rev. Chem.* **2018**, *2*, 82–94. [[CrossRef](#)]
28. Pertot, Y.; Schmidt, C.; Matthews, M.; Chauvet, A.; Huppert, M.; Svoboda, V.; von Conta, A.; Tehlar, A.; Baykusheva, D.; Wolf, J.P.; et al. Time-resolved X-ray absorption spectroscopy with a water window high-harmonic source. *Science* **2017**, *355*, 264–267. [[CrossRef](#)]
29. Teichmann, S.M.; Silva, F.; Cousin, S.L.; Hemmer, M.; Biegert, J. 0.5-keV Soft X-ray attosecond continua. *Nat. Commun.* **2016**, *7*, 11493. [[CrossRef](#)]
30. La Cäer, S. Water Radiolysis: Influence of Oxide Surfaces on H_2 Production under Ionizing Radiation. *Water* **2011**, *3*, 235–253. [[CrossRef](#)]
31. Long, F.H.; Lu, H.; Eisenthal, K.B. Femtosecond studies of the presolvated electron: An excited state of the solvated electron? *Phys. Rev. Lett.* **1990**, *64*, 1469–1472. [[CrossRef](#)] [[PubMed](#)]
32. Migus, A.; Gauduel, Y.; Martin, J.L.; Antonetti, A. Excess electrons in liquid water: First evidence of a prehydrated state with femtosecond lifetime. *Phys. Rev. Lett.* **1987**, *58*, 1559–1562. [[CrossRef](#)] [[PubMed](#)]
33. Crowell, R.A.; Bartels, D.M. Multiphoton Ionization of Liquid Water with 3.0–5.0 eV Photons. *J. Phys. Chem.* **1996**, *100*, 17940–17949. [[CrossRef](#)]
34. Elles, C.G.; Jailaubekov, A.E.; Crowell, R.A.; Bradforth, S.E. Excitation-energy dependence of the mechanism for two-photon ionization of liquid H_2O and D_2O from 8.3 to 12.4 eV. *J. Chem. Phys.* **2006**, *125*, 044515. [[CrossRef](#)] [[PubMed](#)]
35. Silva, C.; Walhout, P.K.; Yokoyama, K.; Barbara, P.F. Femtosecond Solvation Dynamics of the Hydrated Electron. *Phys. Rev. Lett.* **1998**, *80*, 1086–1089. [[CrossRef](#)]
36. Pshenichnikov, M.S.; Baltuška, A.; Wiersma, D.A. Hydrated-electron population dynamics. *Chem. Phys. Lett.* **2004**, *389*, 171–175. [[CrossRef](#)]
37. Marsalek, O.; Elles, C.G.; Pieniazek, P.A.; Pluhařová, E.; VandeVondele, J.; Bradforth, S.E.; Jungwirth, P. Chasing charge localization and chemical reactivity following photoionization in liquid water. *J. Chem. Phys.* **2011**, *135*, 224510. [[CrossRef](#)]
38. Young, L.; Arms, D.A.; Dufresne, E.M.; Dunford, R.W.; Ederer, D.L.; Höhr, C.; Kanter, E.P.; Krässig, B.; Landahl, E.C.; Peterson, E.R.; et al. X-ray Microprobe of Orbital Alignment in Strong-Field Ionized Atoms. *Phys. Rev. Lett.* **2006**, *97*, 083601. [[CrossRef](#)]
39. Goulielmakis, E.; Loh, Z.H.; Wirth, A.; Santra, R.; Rohringer, N.; Yakovlev, V.S.; Zherebtsov, S.; Pfeifer, T.; Azzeer, A.M.; Kling, M.F.; et al. Real-time observation of valence electron motion. *Nature* **2010**, *466*, 739–743. [[CrossRef](#)]
40. Vidal, M.L.; Feng, X.; Epifanovsky, E.; Krylov, A.I.; Coriani, S. New and Efficient Equation-of-Motion Coupled-Cluster Framework for Core-Excited and Core-Ionized States. *J. Chem. Theory Comput.* **2019**, *15*, 3117–3133. [[CrossRef](#)]
41. Li, J.; Nie, Z.; Zheng, Y.Y.; Dong, S.; Loh, Z.H. Elementary Electron and Ion Dynamics in Ionized Liquid Water. *J. Phys. Chem. Lett.* **2013**, *4*, 3698–3703. [[CrossRef](#)]
42. Nagasaka, M.; Hatsui, T.; Horigome, T.; Hamamura, Y.; Kosugi, N. Development of a liquid flow cell to measure soft X-ray absorption in transmission mode: A test for liquid water. *J. Electron. Spectrosc. Relat. Phenom.* **2010**, *177*, 130–134. [[CrossRef](#)]
43. Winter, B.; Weber, R.; Widdra, W.; Dittmar, M.; Faubel, M.; Hertel, I.V. Full Valence Band Photoemission from Liquid Water Using EUV Synchrotron Radiation. *J. Phys. Chem. A* **2004**, *108*, 2625–2632. [[CrossRef](#)]
44. Li, Z.; El-Amine Madjet, M.; Vendrell, O.; Santra, R. Core-level transient absorption spectroscopy as a probe of electron hole relaxation in photoionized $\text{H}^+(\text{H}_2\text{O})_n$. *Faraday Discuss.* **2014**, *171*, 457–470. [[CrossRef](#)]
45. Lutman, A.A.; Coffee, R.; Ding, Y.; Huang, Z.; Krzywinski, J.; Maxwell, T.; Messerschmidt, M.; Nuhn, H.D. Experimental Demonstration of Femtosecond Two-Color X-ray Free-Electron Lasers. *Phys. Rev. Lett.* **2013**, *110*, 134801. [[CrossRef](#)]
46. Lutman, A.A.; Maxwell, T.J.; MacArthur, J.P.; Guetg, M.W.; Berrah, N.; Coffee, R.N.; Ding, Y.; Huang, Z.; Marinelli, A.; Moeller, S.; et al. Fresh-slice multicolour X-ray free-electron lasers. *Nat. Photonics* **2016**, *10*, 745–750. [[CrossRef](#)]
47. Duris, J.; Li, S.; Driver, T.; Champenois, E.G.; MacArthur, J.P.; Lutman, A.A.; Zhang, Z.; Rosenberger, P.; Aldrich, J.W.; Coffee, R.; et al. Tunable isolated attosecond X-ray pulses with gigawatt peak power from a free-electron laser. *Nat. Photonics* **2020**, *14*, 30–36. [[CrossRef](#)]

48. Emma, P.; Bane, K.; Cornacchia, M.; Huang, Z.; Schlarb, H.; Stupakov, G.; Walz, D. Femtosecond and Subfemtosecond X-ray Pulses from a Self-Amplified Spontaneous-Emission-Based Free-Electron Laser. *Phys. Rev. Lett.* **2004**, *92*, 074801. [CrossRef] [PubMed]
49. Chuang, Y.D.; Shao, Y.C.; Cruz, A.; Hanzel, K.; Brown, A.; Frano, A.; Qiao, R.; Smith, B.; Domning, E.; Huang, S.W.; et al. Modular soft X-ray spectrometer for applications in energy sciences and quantum materials. *Rev. Sci. Instrum.* **2017**, *88*, 013110. [CrossRef] [PubMed]
50. Heimann, P.; Reid, A.; Feng, Y.; Fritz, D. Fluorescence intensity monitors as intensity and beam-position diagnostics for X-ray free-electron lasers. *J. Synchrotron Radiat.* **2019**, *26*, 358–362. [CrossRef]
51. Curie, P.; Debierne, A. Sur la radio-activité induite et les gaz activés par le radium. *Compt. Rend* **1901**, *132*, 768–770.
52. Keene, J.P. Kinetics of Radiation-induced Chemical Reactions. *Nature* **1960**, *188*, 843–844. [CrossRef]
53. Matheson, M.S.; Dorfman, L.M. Detection of Short-Lived Transients in Radiation Chemistry. *J. Chem. Phys.* **1960**, *32*, 1870–1871. [CrossRef]
54. McCarthy, R.; MacLachlan, A. Transient benzyl radical reactions produced by high-energy radiation. *Trans. Faraday Soc.* **1960**, *56*, 1187–1200. [CrossRef]
55. Belloni, J.; Monard, H.; Gobert, F.; Larbre, J.P.; Demarque, A.; De Waele, V.; Lampre, I.; Marignier, J.L.; Mostafavi, M.; Bourdon, J.C.; et al. ELYSE—A picosecond electron accelerator for pulse radiolysis research. *Nucl. Instrum. Methods Phys. Res. Sect. A: Accel. Spectrometers Detect. Assoc. Equip.* **2005**, *539*, 527–539. [CrossRef]
56. Wishart, J.F.; Cook, A.R.; Miller, J.R. The LEAF picosecond pulse radiolysis facility at Brookhaven National Laboratory. *Rev. Sci. Instrum.* **2004**, *75*, 4359–4366. [CrossRef]
57. Clark, S.B.; Buchanan, M.; Wilmarth, B. *Basic Research Needs for Environmental Management*; Technical Report; PNNL-25166; DOE: Washington, DC, USA, 2016.
58. Peterson, R.A.; Buck, E.C.; Chun, J.; Daniel, R.C.; Herting, D.L.; Ilton, E.S.; Lumetta, G.J.; Clark, S.B. Review of the scientific understanding of radioactive waste at the US DOE Hanford Site. *Environ. Sci. Technol.* **2018**, *52*, 381–396. [CrossRef]
59. Colburn, H.A.; Peterson, R.A. A history of Hanford tank waste, implications for waste treatment, and disposal. *Environ. Prog. Sustain. Energy* **2020**, *40*, e13567.
60. Kruger, A.A.; Vienna, J.D.; Kim, D.S. *Advances in the Glass Formulations for the Hanford Tank Waste Treatment and Immobilization Plant*; Technical Report; Hanford Site (HNF): Richland, WA, USA, 2015.
61. Page, J.S.; Reynolds, J.G.; Cooke, G.A.; Wells, B.E. Large cemented gibbsite agglomerates in alkaline nuclear waste at the Hanford site and the impacts to remediation. *J. Hazard. Mater.* **2020**, *384*, 121318. [CrossRef]
62. Gephart, R.E. A short history of waste management at the Hanford Site. *Phys. Chem. Earth Parts A/B/C* **2010**, *35*, 298–306. [CrossRef]
63. Gephart, R.E.; Lundgren, R.E. *Hanford Tank Clean Up: A Guide to Understanding the Technical Issues*; Technical Report; Pacific Northwest Lab.: Richland, WA, USA, 1995.
64. Pimblott, S.M.; LaVerne, J.A.; Mozumder, A.; Green, N.J. Structure of electron tracks in water. 1. Distribution of energy deposition events. *J. Phys. Chem.* **1990**, *94*, 488–495. [CrossRef]
65. Pimblott, S.M.; LaVerne, J.A. Stochastic simulation of the electron radiolysis of water and aqueous solutions. *J. Phys. Chem. A* **1997**, *101*, 5828–5838. [CrossRef]
66. PNNL: Tank Waste Information Network System; Best Basis Inventory. 2020. Available online: <https://twins.labworks.org/twinsdata/forms/about.aspx?subject=BestBasisInventory> (accessed on 6 April 2020.)
67. Graham, T.R.; Dembowski, M.; Hu, J.Z.; Jaegers, N.R.; Zhang, X.; Clark, S.B.; Pearce, C.I.; Rosso, K.M. Intermediate Species in the Crystallization of Sodium Aluminate Hydroxy Hydrates. *J. Phys. Chem. C* **2020**, *124*, 12337–12345. [CrossRef]
68. Graham, T.R.; Gorniak, R.; Dembowski, M.; Zhang, X.; Clark, S.B.; Pearce, C.I.; Clark, A.E.; Rosso, K.M. Solid-State Recrystallization Pathways of Sodium Aluminate Hydroxy Hydrates. *Inorg. Chem.* **2020**, *59*, 6857–6865. [CrossRef] [PubMed]
69. Zhang, Y.; Zheng, S.; Du, H.; Wang, S.; Zhang, Y. Solubility of Al₂O₃ in the Na₂O–Al₂O₃–H₂O–CH₃OH System at (30 and 60) °C. *J. Chem. Eng. Data* **2010**, *55*, 1237–1240. [CrossRef]
70. Pimblott, S.M.; LaVerne, J.A.; Bartels, D.M.; Jonah, C.D. Reconciliation of transient absorption and chemically scavenged yields of the hydrated electron in radiolysis. *J. Phys. Chem.* **1996**, *100*, 9412–9415. [CrossRef]
71. Jones, B.M.; Hu, H.; Alexandrov, A.; Smith, W.; Clark, A.E.; Li, X.; Orlando, T.M. Efficient Intermolecular Energy Exchange and Soft Ionization of Water at Nanoplatelet Interfaces. *J. Phys. Chem. Lett.* **2020**, *11*, 10088–10093. [CrossRef]
72. Stumpf, V.; Brunken, C.; Gokhberg, K. Impact of metal ion's charge on the interatomic Coulombic decay widths in microsolvated clusters. *J. Chem. Phys.* **2016**, *145*, 104306. [CrossRef]
73. Norman, P.; Dreuw, A. Simulating X-ray Spectroscopies and Calculating Core-Excited States of Molecules. *Chem. Rev.* **2018**, *118*, 7208–7248. [CrossRef]
74. Besley, N.A. Density Functional Theory Based Methods for the Calculation of X-ray Spectroscopy. *Accounts Chem. Res.* **2020**, *53*, 1306–1315. [CrossRef]
75. Sorensen, S.L.; Zheng, X.; Southworth, S.H.; Patanen, M.; Kokkonen, E.; Oostenrijk, B.; Travnikova, O.; Marchenko, T.; Simon, M.; Bostedt, C.; et al. From synchrotrons for XFELs: The soft X-ray near-edge spectrum of the ESCA molecule. *J. Phys. B At. Mol. Opt. Phys.* **2020**, *53*, 244011. [CrossRef]

76. Zheng, X.; Liu, J.; Doumy, G.; Young, L.; Cheng, L. Hetero-site Double Core Ionization Energies with Sub-electronvolt Accuracy from Delta-Coupled-Cluster Calculations. *J. Phys. Chem. A* **2020**, *124*, 4413–4426. [[CrossRef](#)] [[PubMed](#)]
77. Stanton, J.F.; Bartlett, R.J. The equation of motion coupled-cluster method. A systematic biorthogonal approach to molecular excitation energies, transition probabilities, and excited state properties. *J. Chem. Phys.* **1993**, *98*, 7029–7039. [[CrossRef](#)]
78. Krylov, A.I. Equation-of-Motion Coupled-Cluster Methods for Open-Shell and Electronically Excited Species: The Hitchhiker's Guide to Fock Space. *Annu. Rev. Phys. Chem.* **2008**, *59*, 433–462. [[CrossRef](#)]
79. Cederbaum, L.S.; Domcke, W.; Schirmer, J. Many-body theory of core holes. *Phys. Rev. A* **1980**, *22*, 206–222. [[CrossRef](#)]
80. Coriani, S.; Koch, H. Communication: X-ray absorption spectra and core-ionization potentials within a core-valence separated coupled cluster framework. *J. Chem. Phys.* **2015**, *143*, 181103. [[CrossRef](#)] [[PubMed](#)]
81. Zheng, X.; Cheng, L. Performance of Delta-Coupled-Cluster Methods for Calculations of Core-Ionization Energies of First-Row Elements. *J. Chem. Theory Comput.* **2019**, *15*, 4945–4955. [[CrossRef](#)] [[PubMed](#)]
82. Nanda, K.D.; Vidal, M.L.; Faber, R.; Coriani, S.; Krylov, A.I. How to stay out of trouble in RIXS calculations within equation-of-motion coupled-cluster damped response theory? Safe hitchhiking in the excitation manifold by means of core-valence separation. *Phys. Chem. Chem. Phys.* **2020**, *22*, 2629–2641. [[CrossRef](#)] [[PubMed](#)]
83. Hao, Y.; Inhester, L.; Hanasaki, K.; Son, S.K.; Santra, R. Efficient electronic structure calculation for molecular ionization dynamics at high X-ray intensity. *Struct. Dyn.* **2015**, *2*, 041707. [[CrossRef](#)] [[PubMed](#)]
84. Ho, P.J.; Daurer, B.J.; Hantke, M.F.; Bielecki, J.; Al Haddad, A.; Bucher, M.; Doumy, G.; Ferguson, K.R.; Flückiger, L.; Gorkhovor, T.; et al. The role of transient resonances for ultra-fast imaging of single sucrose nanoclusters. *Nat. Commun.* **2020**, *11*, 167. [[CrossRef](#)]
85. Serkez, S.; Decking, W.; Froehlich, L.; Gerasimova, N.; Grünert, J.; Guetg, M.; Huttula, M.; Karabekyan, S.; Koch, A.; Kocharyan, V.; et al. Opportunities for Two-Color Experiments in the Soft X-ray Regime at the European XFEL. *Appl. Sci.* **2020**, *10*, 728. [[CrossRef](#)]
86. Reiche, S.; Knopp, G.; Pedrini, B.; Prat, E.; Aeppli, G.; Gerber, S. Towards the Perfect X-ray Beam Splitter. *arXiv* **2020**, arXiv:physics.acc-ph/2010.00230.
87. Engel, R.; Miedema, P.; Turenne, D.; Vaskivskyi, I.; Brenner, G.; Dziarzhytski, S.; Kuhlmann, M.; Schunck, J.; Döring, F.; Styervoyedov, A.; et al. Parallel Broadband Femtosecond Reflection Spectroscopy at a Soft X-ray Free-Electron Laser. *Appl. Sci.* **2020**, *10*, 6947. [[CrossRef](#)]
88. Schlotter, W.F.; Beye, M.; Zohar, S.; Coslovich, G.; Dakovski, G.L.; Lin, M.F.; Liu, Y.; Reid, A.; Stubbs, S.; Walter, P.; et al. Balanced Detection in Femtosecond X-ray Absorption Spectroscopy to Reach the Ultimate Sensitivity Limit. *arXiv* **2020**, arXiv:physics.ins-det/2006.13968.